The ac Hall effect in high-T_c superconductors

The ac Hall effect in high-T_c superconductors

H D Drew, S Wu and H-T S Lihn

Laboratory for Physical Sciences, College Park, MD 20740, and Center for Superconductivity Research, Department of Physics, University of Maryland, College Park, MD 20742, USA

Abstract. Far-infrared magnetotransmission measurements of normal-state $YBa_2Cu_3O_7$ thin films are discussed. The magneto-optical signals observed in circularly polarized light are consistent with the ac Hall effect of holes with a reduced scattering rate and an enhanced mass compared to the zero-field transport parameters. The results agree with a simple high-frequency extension of models which have been developed to explain the anomalous dc Hall effect in the normal state of high-T_c superconductors in terms of two scattering rates. The Hall scattering rate $1/\tau_H \sim T^n/W_s$, where $n \geqslant 2$ and $W_s \cong 120$ K. These experiments provide new tests of the Fermi-liquid versus non-Fermi-liquid nature of these materials.

1. Introduction

Dc transport in the *ab*-plane in the normal state of high-temperature superconductors is anomalous and has been cited as evidence for the non-Fermi-liquid nature of these strongly interacting metals [1]. The temperature dependence of the resistivity is linear to temperatures well above room temperature and shows no sign of saturation. Hall measurements have revealed the charge carriers to be holes with a density related to the oxygen doping level, but there the resemblance to simple metals ends. A striking T^2-behaviour of the inverse Hall angle, cot $\theta_H = \sigma_{xx}/\sigma_{xy}$, has been observed over a wide temperature range in many different materials and types of sample [2–5]. In addition, the ac conductivity, derived from broad-band optical reflectivity measurements [6, 7], shows distinctly non-Drude-like behaviour above 200 cm^{-1}.

In this paper we discuss measurements of the far-infrared (FIR) magneto-optical activity of $YBa_2Cu_3O_7$ thin films in the normal state in fields up to 9 T where $\omega_c\tau \sim 1/40$, so that we observe the weak-field ac Hall effect [8]. The signal is consistent with a hole-like Hall effect, but fitting the data to a Drude model requires a smaller scattering rate and larger mass than the zero-field values. This result is understood by extending the ideas of Anderson (see [2, 3]) or Carrington *et al* (see [4, 5]), used to explain the temperature dependence of the dc Hall effect, to high frequencies. In these theories, the Hall effect is dependent upon a scattering time and mass which are distinct from the ordinary transport quantities. In Anderson's Luttinger-liquid picture these parameters are associated with spinon excitations, whereas in the Fermi-liquid theories they are the relaxation times and effective masses associated with the carriers near the corners of the 2D Fermi surface. Other theories have also been proposed to explain the appearance of two scattering times in the charge dynamics of cuprate materials [9–11]. We conclude with a discussion of the prospects for these ac Hall measurements to resolve the Fermi-liquid/non-Fermi-liquid question for the normal state of high-temperature superconductors.

2. Experimental details

The samples were high-quality films of $YBa_2Cu_3O_7$ grown on Si or $LaAlO_3$ substrates by pulsed laser ablation [8]. Far-infrared magnetotransmission measurements from 10 to 200 cm^{-1}, in the Faraday geometry, were performed with a polarizing Michelson interferometer above 30 cm^{-1}, and with several lines from an optically pumped FIR laser below 55 cm^{-1}, in conjunction with a 4.2 K Si bolometric detector. The samples were held in the bore of a superconducting 9 T magnet on a movable stage, allowing the temperature to be varied from 4 K to 200 K and the transmission of a sample to be compared to that of a blank substrate for absolute transmission measurements. A circular polarizer, consisting of a linear polarizer and an x-cut quartz waveplate, was calibrated using cyclotron resonance in GaAs and InAs quantum well structures [12]. The magneto-optical activity of the samples was 'unfolded' from the raw signal using the measured polarizer calibration curve, as described elsewhere [13].
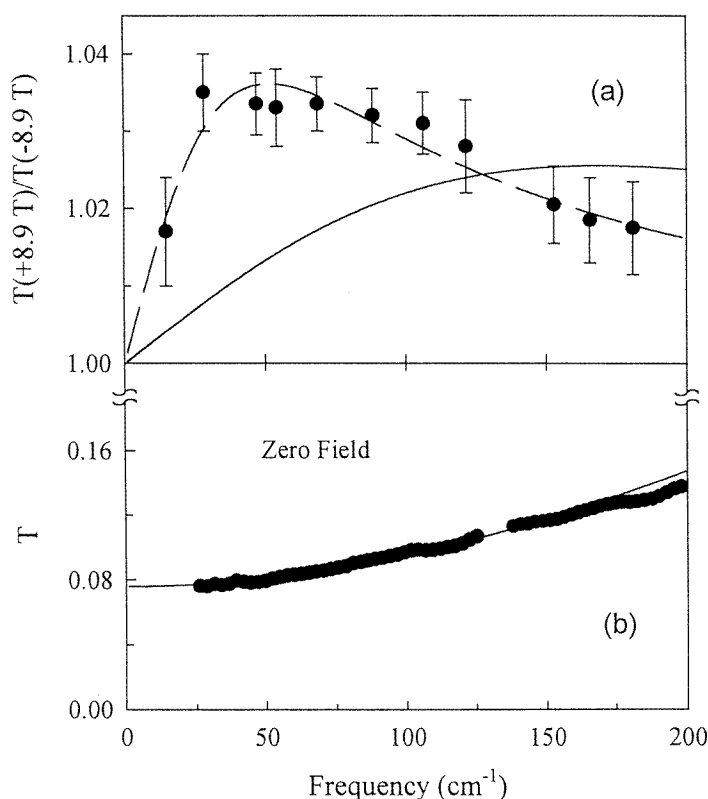

Figure 1. FIR transmission spectra for a 400 Å $YBa_2Cu_3O_7$ film on Si at 95 K. (a) The ratio of the transmittance at +8.9 T to that at −8.9 T with circularly polarized light. The solid circles show the data; the solid line is the prediction of the Drude model with parameters used to fit the zero-field data in (b), and the dashed line is a fit to the modified conductivity form of equation (3). (b) The zero-field transmittance of the sample ratioed to that of a bare substrate. The solid circles are the data, and the solid curve a fit to a Drude conductivity with the parameters listed in the text.

The transmission of the thin-film samples is given by a modified Fresnel formula:

$$T \propto |n + 1 + Z_0\sigma|^{-2} \approx |Z_0\sigma|^{-2} \tag{1}$$

where n is the substrate index, Z_0 the free-space impedance, σ the film conductance. The last identity holds when $Z_0\sigma \gg n$ which is close to the experimental situation. In a magnetic field the ratio T^+/T^- of the transmission for the left-hand and right-hand circular modes was measured:

$$\frac{T(+H)}{T(-H)} = \left| \frac{1 + n + Z_0\sigma^-}{1 + n + Z_0\sigma^+} \right|^2 \approx 1 + 4\,\mathrm{Im}\,\theta_H \tag{2}$$

where $\sigma^{\pm} = \sigma_{xx} \pm i\sigma_{xy}$ is the conductivity function for circularly polarized light and $\theta_H = \tan^{-1}(\sigma_{xy}/\sigma_{xx})$ is the complex frequency-dependent Hall angle, and where the weak-field condition, $\sigma_{xy} \ll \sigma_{xx}$ is also assumed for the last identity in equation (2).

3. Results

Figure 1(a) shows as the solid circles the transmittance ratio $T(+8.9\ \mathrm{T})/T(-8.9\ \mathrm{T})$ in circularly polarized light for a YBa$_2$Cu$_3$O$_7$ film of thickness $d_f = 400\ \text{Å}$ on Si at 95 K. Figure 1(b) shows the zero-field transmission relative to a blank silicon wafer. The gaps in each frame near 130 cm^{-1} are due to a phonon in the quartz waveplate. The magneto-optical activity spectrum in figure 1(a) has a peak near 60 cm^{-1}, while the zero-field spectrum shows a characteristic Drude frequency dependence. The solid curves in each frame show fits to a simple Drude model (using the standard sheet conductance formula for the film and treating the multiple reflections in the substrate incoherently) for a dc sheet resistance $R_\square$ of 25.9 Ω and scattering rate $\tau_{tr}^{-1} = 190$ cm^{-1}. This is the minimum value for τ_{tr}^{-1} that is consistent with the zero-field data. In this fit, we have chosen the carrier mass $m_{tr} = 3.0$ from previous estimates of FIR measurements [13]. However, varying the carrier mass only changes the amplitude, not the peak position of the fit in figure 1(a). In frame 1(b), the Drude curve provides an excellent fit, with the small structures near 120, 155, and 190 cm^{-1} probably coming from optic phonons in YBa$_2$Cu$_3$O$_7$. However, the solid curve in figure 1(a) has a peak near 170 cm^{-1} in contrast to the data which have a peak near 60 cm^{-1}. Therefore, the data in figure 1 show directly that the Hall response is characterized by a relaxation frequency different to that for the zero-field transport currents.

Similar measurements have been made on YBa$_2$Cu$_3$O$_7$ films grown on LaAlO$_3$ substrates [8]. The $T(+H)/T(-H)$ data for one of these films are shown in figure 2. In these films $\tau_{tr}^{-1} \cong 130$ cm^{-1} which is somewhat smaller, consistent with the higher quality of films grown on LaAlO$_3$, while the peak in $T(+H)/T(-H)$ is somewhat higher which arises partly from the higher sample temperature of this trace. In both kinds of sample, the magneto-optical activity $(T^+/T^- - 1)$ shows an approximately Drude-like frequency response, but with a smaller scattering rate than that of the zero-field conductivity.

4. Discussion

These seemingly anomalous results can be understood by using a high-frequency extension of models which have been used to explain the T^2-dependence of the normal-state inverse Hall angle, σ_{xx}/σ_{xy}, observed in dc transport measurements. In Anderson's Luttinger-liquid model [2] for the normal state of high-T_c superconductors, σ_{xx} has the ordinary form, $\propto \tau_{tr}$, the decay time for holons scattering from thermally excited spinons. On the other hand, σ_{xy} depends on both τ_{tr} and the scattering time of spinon excitations, τ_H: $\sigma_{xy} \propto \tau_{tr}\tau_H$.
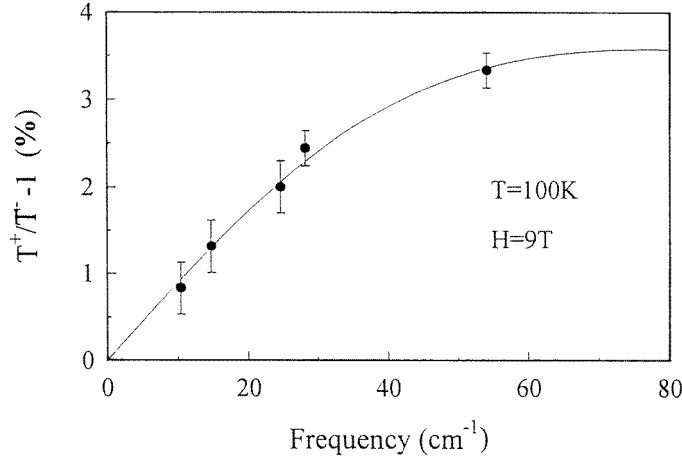
Figure 2. The FIR transmission ratio spectra of the transmittance at $+8.9$ T with respect to that at -8.9 T with circularly polarized light for a 500 Å $YBa_2Cu_3O_7$ film on $LaAlO_3$ at 100 K. The solid circles show the data; the solid line is the prediction of the Anderson–Ong model with $\omega_H = 1.4$ cm^{-1} and $1/\tau_H = 77$ cm^{-1}.

The decay rate for holons, τ_{tr}^{-1}, depends on the number of thermally excited spinons, and so is proportional to T, while the scattering rate for spinons, τ_H^{-1}, depends upon magnetic impurity and spinon–spinon scattering, and goes like $Ax + BT^2$, where x is the concentration of magnetic impurities. This form of the conductivity was used by Ong and co-workers to interpret the dc magnetotransport data [3].

An alternative model, put forward by Carrington *et al* (see [4, 5]) explains the same temperature dependence within a Fermi-liquid model involving Fermi surface (FS) anisotropy in the *ab*-plane. In their model it is assumed that $l_1 \gg l_2$, where l_1 and l_2 are the mean free paths at the corners and along the edges of the FS. In this limit $\sigma_{xx} \propto l_2$ (if the length of the edges is much larger than the corners) and $\sigma_{xy} \propto l_2 l_1$, which leads to the same form as above and the same temperature dependence if $l_1 \propto T^{-2}$ and $l_2 \propto 1/T$ are also assumed.

It is not clear how to extend either of these models to finite frequency in a rigorous manner [8, 14]. The simplest phenomenological approach is to replace τ_H and τ_{tr} in the expressions for σ_{xx} and σ_{xy} with $\tau_H^* = \tau_H/(1 - i\omega\tau_H)$ and $\tau_{tr}^* = \tau_{tr}/(1 - i\omega\tau_{tr})$, respectively. This form is easily justified in the Fermi-liquid models. In the case of two-excitation models such as Anderson's it may result from two coupled Boltzmann equations. This leads to the following weak-field conductivity function:

$$\sigma_\pm \equiv \sigma_{xx} \pm i\sigma_{xy} = \frac{n_c e^2 \tau_{tr}^*}{m_{tr}} \left[1 \pm i\omega_H \tau_H^*\right] \tag{3}$$

where n_c is the carrier density, m_{tr} is the transport mass (for motion perpendicular to the FS in the Anderson model), and $\omega_H = eH/(m_H c)$, with a Hall mass m_H (for motion parallel to the FS). This function reduces to Anderson's or the anisotropic Fermi-liquid result at zero frequency, a simple Drude model if $\tau_H = \tau_{tr}$ and $m_H = m_{tr}$, and obeys causality and the oscillator strength sum rule. The form in equation (3), however, predicts a non-Drude form of the ac Hall signal, with a roll-off frequency for θ_H given by $1/\tau_H$, distinct from the decay rate for the zero-field transport currents, $1/\tau_{tr}$.

The dashed line in figure 1(a) shows a fit to the conductivity function of equation (3) with $\tau_H^{-1} = 52 \pm 10$ cm^{-1} and $m_H = (6.6 \pm 0.8)m_e$, indicating that $\tau_H \sim 4\tau_{tr}$ and $m_H \sim 2m_{tr}$. This fit can be taken as direct evidence for the presence of two distinct scattering rates in the normal-state electrodynamics of YBa$_2$Cu$_3$O$_7$, with the scattering rate associated with the ac Hall effect being much smaller than the transport scattering rate. Within the Anderson picture, we can interpret the parameters m_H and τ_H as the spinon mass and scattering time, respectively.
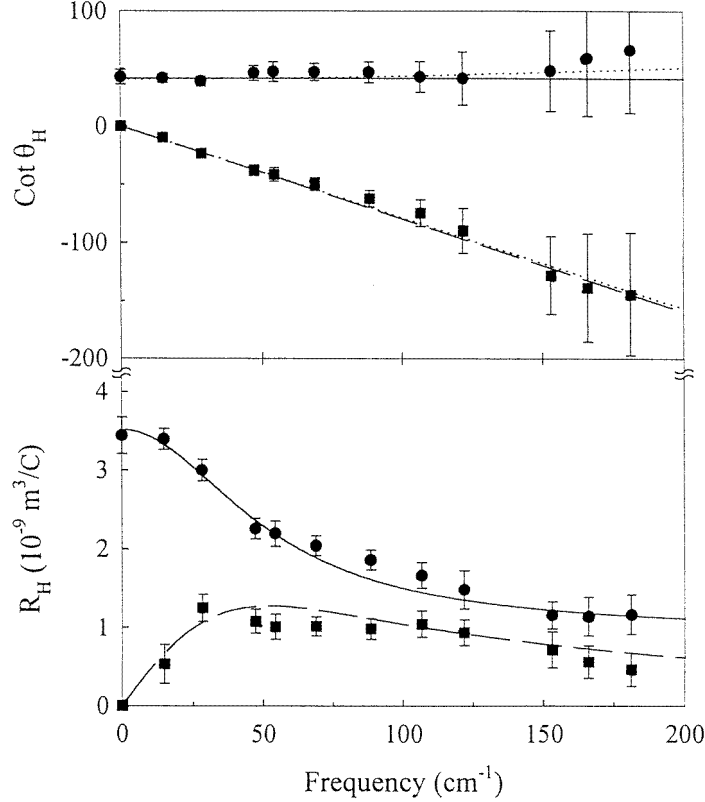

Figure 3. The Hall coefficient, R_H, versus frequency for the Si substrate sample. In the lower panel the solid circles and squares show respectively the real and imaginary parts of R_H derived from Kramers–Kronig analysis of the data in figure 1(a), while the solid and dashed curves show the predicted values from fitting equation (3) to the same data. The real (circles) and imaginary (squares) parts of cot θ_H, along with the predictions of equation (3) (solid and dashed lines) are shown in the upper panel. The real part is $1/(\omega_H \tau_H)$, and the slope of the imaginary part is $-1/\omega_H$.

An alternative to fitting the data in figure 1(a) with the Anderson–Ong conductivity (equation (3)) is to derive the Hall conductivity by applying Kramers–Kronig analysis to the transmission data. In our case the field ratio $T(H)/T(0)$ for unpolarized light (obtained from averaging the two circular polarizations) is different from one by less than 2%, as can be seen in figure 4—see later. Therefore we can conclude that σ_{xx} is almost unchanged from the zero-field value, and use the zero-field σ_{xx} evaluated from analysis of the zero-field transmission data. This σ_{xx} together with a Kramers–Kronig analysis of the $T(+H)/T(-H)$

data then gives σ_{xy} through equation (2).

The results of this analysis are shown in figure 3 in terms of the real (solid circles) and imaginary (solid squares) parts of the Hall coefficient, R_H. We have tried several high-frequency extrapolations for the Kramers–Kronig analysis and found little effect on the overall shape of the R_H-curves below 150 cm^{-1}. In a simple Drude metal, the real part of R_H is frequency independent, given by $1/(n_c ec)$, and the imaginary part is zero. The clear frequency dependence of both quantities in our data is an indication of the non-Drude (and possibly the non-Fermi-liquid) character of the charge dynamics in a magnetic field for this material.

Also shown in figure 3 as the solid and dashed lines are the real and imaginary parts of R_H obtained from equation (3) with the parameters used to fit the data in figure 1. These fits are sensitive to the product $n_c d_f$, and the effective film thickness is known to only ~25%. We obtain a value of 3.5×10^{-9} m^3 C^{-1} for R_H at zero frequency and 95 K which is comparable to published values for the dc Hall coefficient of single-crystal YBa$_2$Cu$_3$O$_7$ with 1% Co impurity [4] and the canonical value of 2.9×10^{-21} cm^{-3} for n_c corresponding to 0.25 holes per in-plane Cu. The fit to both components of R_H is as good as the fit to the transmission data in figure 2, providing a consistency check of both the model and the Kramers–Kronig analysis procedure. We note that the high-frequency limit of equation (3) yields $R_H(\omega \rightarrow \infty) = (m_{tr}/m_H)/(n_c ec)$ which may be used to yield, within the conductivity model, a value for the carrier density, which can only be guessed from the dc Hall effect data. More generally the ac Hall effect is independent of the electron scattering for $\omega\tau \gg 1$ and R_H becomes a fundamental property of the Fermi surface for $\hbar\omega$ greater than the characteristic interaction energies [15, 16].

Figure 3 shows the real and imaginary parts of $\cot\theta_H \approx \theta_H^{-1}$ derived for the Si substrate sample. The real part is almost constant within experimental errors, and is equal to $(\omega_H\tau_H)^{-1}$ from equation (3). Our value of $\omega_H\tau_H = 1/40$ agrees well with the published dc Hall angle data [3, 4]. The imaginary part of θ_H^{-1} is given by $-\omega/\omega_H$, from which we derive $m_H = 6.6m_e$, in agreement with the values fitted to equation (3). The frequency independence of Re$(\cot\theta_H)$ and the linear frequency dependence of Im$(\cot\theta_H)$ are also found in the simple Drude model and in some other models as well [9, 10] with the exception of arbitrary two-band models. We take the values for m_H and τ_H derived from this plot as phenomenological definitions.

5. Temperature dependence

To examine the temperature dependence of $1/\tau_H$ we have measured T^+/T^- over the temperature range from 95 to 140 K at several different laser frequencies for samples of YBa$_2$Cu$_3$O$_7$ grown on LaAlO$_3$. The results are shown in figure 4 where it is seen that the Hall signal is a rapid function of temperature. These data also show that there is a small magnetic-field-induced change in the average magnetotransmission over this temperature and frequency range. This effect corresponds to a magnetoresistance, i.e., a small change in σ_{xx}.

We first discuss the Hall signal. Since the optical data for these films grown on LaAlO$_3$ do not cover a sufficient frequency range to permit a full Kramers–Kronig analysis we have used a curve fitting based on the more complete results at 95 K on the YBCO/Si film. Here we assume the Anderson–Ong form for the conductivity, fix the value of ω_H at 1.2 cm^{-1} (corresponding to $m_H = 7m_e$) and use the transmission data to determine $1/\tau_H$. The results are not very sensitive to ω_H since ω_H affects only the amplitude of θ_H and not its frequency dependence. The results for the 28 and 54 cm^{-1} laser lines are shown in figure 5 where
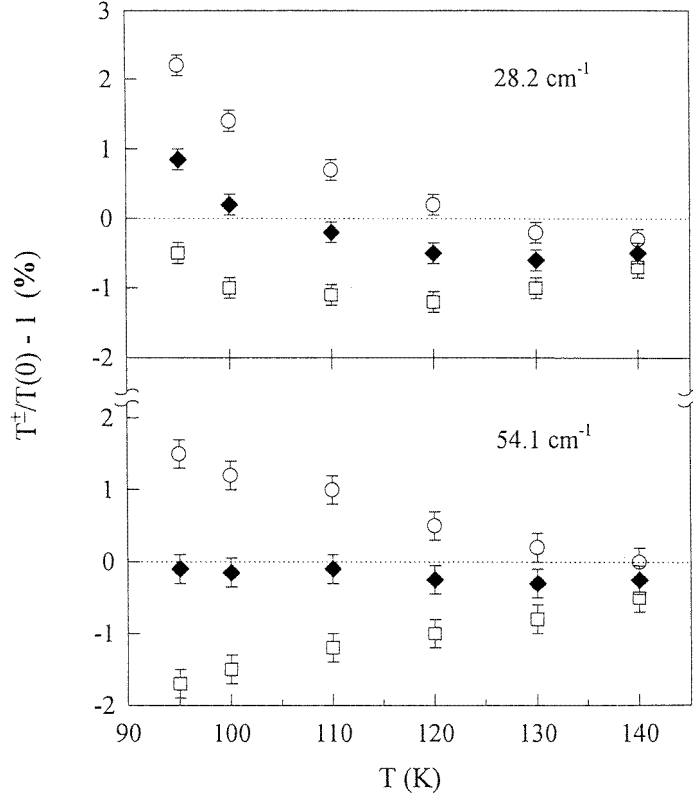
Figure 4. The temperature dependence of $T^+/T_0 - 1$ for the on-LaAlO$_3$ sample of figure 2 at 8.9 T for two different laser wavelengths. The open circles (squares) are for T^+ (T^-). The solid diamonds are the average values.

$1/\tau_H$, plotted against T^2, is seen to be consistent with a temperature dependence T^n with $n \geqslant 2$. Although the deviant behaviour at the highest temperature is systematic and suggests $n > 2$, the measurement errors at these temperatures are large. A power law with $n < 2$ is precluded, however, by the observation that the corresponding best-fit line would have a negative intercept at $T = 0$. Although these results are consistent within the errors of the dc transport, improved high-temperature data over a wider frequency range will be required to adequately test the different models for the magnetotransport of these materials.

The experiment measures $1/\tau_H$, and both transport and FIR results show that the temperature dependence is approximately T^2. Writing $1/\tau_H \cong T^2/W_s$, we find $W_s \cong 120$ K which is surprisingly small. In Fermi-liquid theory W_s is, to within a dimensionless constant, a characteristic energy such as the band width or Fermi energy or the interaction energy. Since these characteristic energies in YBa$_2$Cu$_3$O$_7$ are much larger than the measured W_s we must assume that the dimensionless constant is large. Moreover, these results imply that for the excitation energy $\Delta E \cong \pi^2 W_s$, $\Delta E \cong 1/\tau_H$ and Fermi-liquid theory breaks down.
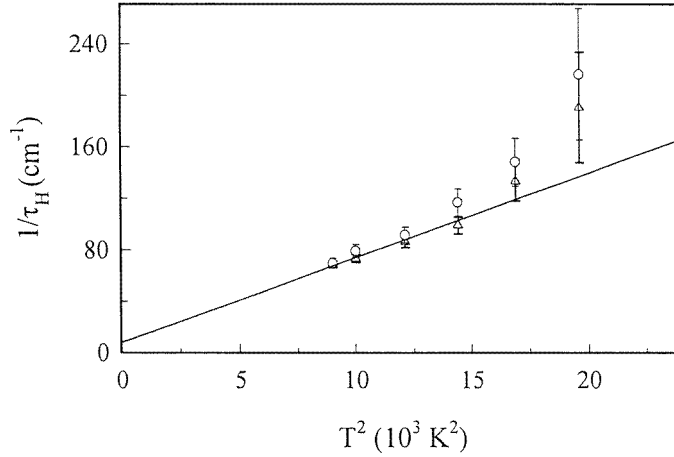
Figure 5. $1/\tau_H$ plotted against T^2 based on an analysis of the data of figure 4. The solid curve is the best fit to $1/\tau_H = T^2/W_s$.

6. Magnetoresistance

The unpolarized transmission at 28 cm^{-1} in figure 4 is seen to be enhanced up to 110 K and then suppressed at higher temperatures by the application of a 9 T magnetic field. The effect is practically unmeasurable at 54 cm^{-1}. Similar effects have been obtained by Liu *et al* from broad-band measurements in magnetic fields up to 27 T where the signal is much larger [17]. They observe that the magnetoresistance signal vanishes above 100 cm^{-1}. Therefore, this effect has a strong frequency and temperature dependence. The semiclassical magnetoresistance, which would be of order $(\omega_c\tau)^2$ is far too small to account for this ac magnetoresistance. Rather it is more likely that this effect results from the magnetic field suppression of the superconducting fluctuations in the normal state at these temperatures close to T_c. At low frequencies the superconducting fluctuations lead to a reduction in the resistivity [18]. The existing theories predict that these effects are suppressed at finite frequencies or magnetic fields [19]. This would lead to a magnetic-field-induced enhancement of the resistivity and, therefore, the transmission in contrast to the observed suppression ($T > 110$ K). While this effect is not understood, we propose that it represents a frequency dependence of the paraconductivity different to that expected and found in experiments for $\omega < \omega_c$. The data suggest that the paraconductivity may become negative when $\omega > \omega_c$. That is, a cyclotron resonance of the paraconductivity may be implied. Indeed, the right sign of the effect is found if it is assumed that the paraconductivity is dominated by long-lived quasiparticles such that $\omega\tau_{qp} > 1$. However, the observed magnitude of $\delta\sigma_{xx}$ is too large to be consistent with this simple picture since superconducting fluctuations of size $R_c \cong \omega_c/v_F \gg \xi$ are required, where R_c is the cyclotron radius and ξ is the superconducting coherence length.

7. The Hall angle sum rule

The Hall angle $\theta_H = \sigma_{xy}/\sigma_{xx}$ has the analytic properties of a response function, so it satisfies the Kramers–Kronig relations [15]. At high frequencies the electron dynamics

becomes interaction free and θ_H approaches a well defined value of the form $\theta_H = i\omega_H/\omega$ where ω_H is the 'Hall frequency' which can be expressed as the ratio of two integrals over the Fermi surface [15]. Therefore the high-frequency limit of the Kramers–Kronig relations gives rise to a sum rule on the real part of θ_H:

$$\int_0^\infty \mathrm{Re}\,\theta_H\ \mathrm{d}\omega = \frac{\pi}{2}\omega_H. \tag{4}$$
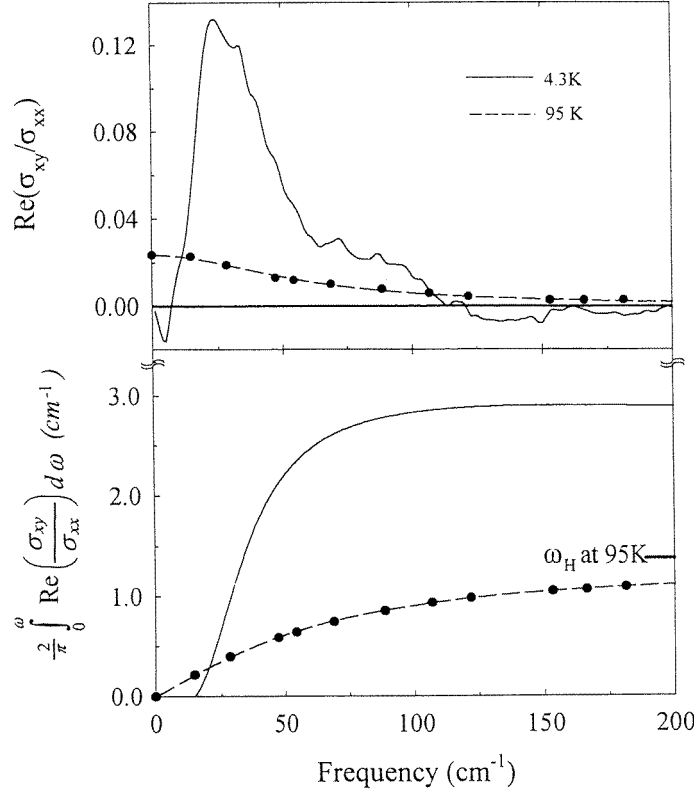
Figure 6. The top panel shows the Hall angle as a function of frequency for the superconducting state at $T = 4.2$ K (solid line) and the normal state at 95 K of the YBa$_2$Cu$_3$O$_7$ film on Si. The magnetic field is 9 T. The lower panel shows the Hall angle sum for the two cases. The horizontal tick on the right-hand side marks the high-frequency limit of the normal-state Hall sum based on an extrapolation using the Anderson–Ong conductivity function.

One important property of this sum rule is that it is independent of temperature or thermodynamic state. Therefore equation (4) must give the same result in the normal and superconducting states. In figure 6, top panel, we show $\mathrm{Re}\,\theta_H$ in the superconducting and normal states for a sample of YBCO grown on Si. For the superconducting state θ_H is dominated by a hybridized pinning-cyclotron resonance in the hole-active sense of circularly polarized light [20]. This leads to a much larger Hall angle for the superconducting state over the measured spectral range. The Hall angle integrals for superconducting and normal states are shown in figure 6, bottom panel. It is seen that both integrals appear to be converging but to different values. Also, the Hall sum seems to be converging more

rapidly in the superconducting state, consistent with reduced damping in the superconducting state. The asymptotic values correspond to effective masses of $3.1m_e$ and $6.8m_e$ for the superconducting and normal states respectively. Similar values are also found directly from the high-frequency behaviour of the optical activity data, $T^+/T^- - 1 \approx 4\,\mathrm{Im}\,\theta_H = 4\omega_c/\omega$ for $\omega\tau \gg 1$. The sum rule implies that there is spectral weight in the Hall angle at frequencies above our measurement limit. Whether this corresponds to too little Hall weight in the normal state or too much in the superconducting state (the Hall angle can change sign) is a question that awaits magneto-optical studies of these materials at higher frequencies.

8. Frequency-dependent scattering

One interesting interpretation of the discrepancy in the Hall angle sum rule is that the normal-state Hall angle has a high-frequency tail. This is not precluded by the existing experimental data, within the limitations of the Kramers–Kronig analysis. Also, if $1/\tau_H$ varies as T^2, an ω^2-dependence is also expected on general grounds leading naturally to a high-frequency tail in θ_H. In order to explore this possibility we have adapted the frequency-dependent relaxation rate formalism that is commonly used for the analysis of the conductivity of electron systems with inelastic scattering processes [21]. We take a generalized Hall angle of the form

$$\theta_H = \frac{\omega_{sc}}{\mathrm{i}\omega + \Gamma(\omega)} \tag{5}$$

where ω_{sc} is the superconducting value. For the complex frequency-dependent relaxation rate $\Gamma(\omega)$ we take the simplest non-trivial form consistent with the T^2 and ω^2 low-frequency behaviour and saturation at high frequencies:

$$\Gamma(\omega) = AT^2 + \lambda_0 \frac{\omega\omega_0}{\omega - \mathrm{i}\omega_0} \tag{6}$$

where λ_0 is the zero-frequency mass-enhancement factor and ω_0 is a characteristic saturation frequency for inelastic scattering processes. λ_0 and ω_0 are chosen such that θ_H approaches the simple generalized Anderson form at low frequency, $\theta_H = \omega_H/(\mathrm{i}\omega + 1/\tau_H)$ with $\omega_H = \omega_{sc}(1+\lambda_0)^{-1}$ and $1/\tau_H = ((2\pi T)^2 + \omega^2)/((2\pi)^2 W_s)$ as expected for the conductivity in Fermi-liquid theory [22]. This leads to $\lambda_0 = 1.1$ and $\omega_0 = 2400$ K. The resulting R_H-curve is shown as dotted lines in figure 3. It is seen that this generalization of the ac Anderson–Ong conductivity, which satisfies the Hall angle sum rule by construction, is not inconsistent with the data. A characteristic energy for the fermion interactions is suggested by these results of order $\omega_0 \sim J$, the antiferromagnetic exchange energy. However interesting these observations, they are supported by few or no data at this point and will clearly require studies at higher frequency to validate.

9. Fermi-liquid models

Several authors have proposed that the anomalous magnetotransport in high-temperature superconductors may be understood in terms of conventional transport within an anisotropic Fermi-liquid theory [4, 5, 16]. Indeed this provides a natural way to introduce multiple-scattering rates. In the model given by Carrington *et al* that was mentioned earlier it was proposed that in the (π, π) direction, the scattering rate $1/\tau_1$ was small and varies as T^2 while the Fermi velocity v_1 is high, whereas in the $(\pi, 0)$ directions where the Fermi surface is flat, the scattering rate is larger and varies as T and the Fermi velocity v_2 is small. If these conditions hold so that $l_1 \gg l_2$, and yet l_2 dominates σ_{xx} (because of the large size of

the flat portions of the Fermi surface), the Anderson–Ong form of the conductivity follows. However, these conditions do not appear to hold near T_c in these materials. Interpreting the parameters in terms of l_1 and l_2 in the anisotropic FS model, we conclude that the two mean free paths differ by only ∼50%, which seems to violate the geometric constraint used to motivate this picture [23]. More importantly, these assumptions would become less valid at higher temperatures.

On the other hand the observed magnetotransmission data can be well described in terms of a general two-band model [16]:

$$\sigma_{xx} = A_1\tau_1 + A_2\tau_2 \tag{7a}$$
$$\sigma_{xy} = B_1\tau_1^2 + B_2\tau_2^2 \tag{7b}$$

where A_i and B_i are constants which can be expressed as integrals over the two parts of the Fermi surface where the scattering times are τ_i ($i = 1, 2$). The results of a best fit of the magnetotransmission data to this model fit the data in figures 1 and 3 just as well as the ac Anderson–Ong conductivity [16]. The corresponding temperature dependence at $\omega = 0$, assuming $1/\tau_1 \propto T^2$ and $1/\tau_2 \propto T$, is also qualitatively consistent with the magnetotransport data. The resistivity is nearly linear in T while the inverse Hall angle varies with a power law somewhat less than T^2. However, this fit also does not appear to be consistent with the Fermi surface observed in angular resolved photoemission [23, 16]. Finally, we note that obtaining $\mathrm{Im}\,\theta_H^{-1} \propto \omega$ with a constant slope, within this model, requires a relation between the A- and B-coefficients and the scattering times which can only hold at one temperature. This suggests that the temperature dependence of the ac Hall effect may permit a discrimination between the Fermi-liquid and non-Fermi-liquid models that have been proposed for the anomalous magnetotransport in high-T_c materials.

10. Conclusions

The ac Hall effect in $YBa_2Cu_3O_7$ supports the two-relaxation-time picture suggested by the dc transport and allows a direct measurement of the τs. The Hall scattering rate $\tau_H^{-1} \cong T^2/W_s$ with $W_s \cong 120$ K, which seems surprisingly small, since the T^2-dependence of the dc Hall angle is observed to persist to above room temperature. An ac generalization of the Anderson–Ong conductivity provides the simplest empirical description of the magneto-optical data. The experiment raises the prospect of a definitive discrimination between Fermi-liquid and non-Fermi-liquid models of the *ab*-plane charge transport in these strongly interacting metals by extending the measurements to higher temperatures and frequencies. In particular, it appears that ac Hall measurements in the $\omega \sim J$ frequency region may be particularly informative.

Significant improvements in the measurement sensitivity are possible and necessary for further progress. Improving the laser stability will permit approximately one order of magnitude improvement in the signal-to-noise ratio. An additional order of magnitude can be achieved by using polarization modulation techniques at all frequencies.

Acknowledgments

References

[1] Anderson P W 1992 *Science* **256** 1526
[2] Anderson P W 1991 *Phys. Rev. Lett.* **67** 2092
[3] Chien T R, Wang Z Z and Ong N P 1991 *Phys. Rev. Lett.* **67** 2088
    Harris J M, Yan Y F and Ong N P 1992 *Phys. Rev.* B **46** 14 293
[4] Carrington A, Mackenzie A P, Lin C T and Cooper J R 1992 *Phys. Rev. Lett.* **69** 2855
[5] Kendziora C, Mandrus D and Mihaly L 1992 *Phys. Rev.* B **46** 14 297
[6] Orenstein J, Thomas G A, Millis A J, Cooper S L, Rapkine D H, Timusk T, Schneemeyer L F and
    Waszczak J V 1990 *Phys. Rev.* B **42** 6342
[7] Rotter L D, Schlesinger Z, Collins R T, Holtzberg F, Field C, Welp U W, Crabtree G W, Liu J Z, Fang Y,
    Vandervoort K G and Fleshler S 1991 *Phys. Rev. Lett.* **67** 2741
[8] Kaplan S G, Wu S, Lihn H-T S, Drew H D, Qi Li, Fenner D, Philips J M and Hou S Y 1996 *Phys. Rev.
    Lett.* **76** 696
[9] Coleman P, Schofield A J and Tsvelik A M 1996 *Phys. Rev. Lett.* **76** 1329
[10] Kotliar G, Sengupta A and Varma C M 1996 to be published
[11] Stojković B P and Pines D 1996 *Phys. Rev. Lett.* **76** 811
[12] Wu S, Kaplan S G, Quijada M, Sengupta K and Drew H D 1995 *Rev. Sci. Instrum.* **66** 5559
[13] Karrai K, Choi E, Dunmore F, Liu S, Ying, X, Qi Li, Venkatesan T and Drew H D 1992 *Phys. Rev. Lett.* **69**
    355
[14] Romero D B 1992 *Phys. Rev.* B **46** 8505
[15] Drew H D and Coleman P 1996 cond-mat/9609010 to be published
[16] Zheleznyak V A, Yakovenko V and Drew H D 1996 to be published
[17] Liu H L, Zibold A, Tanner D B, Li M Y, Wu M K and Wang Y J 1996 to be published
    The larger signal observed by these authors is consistent with $\delta\sigma_{xx} \propto H^2$.
[18] Friedmann T A, Rice J P, Giapintzakis J and Ginsberg D M 1989 *Phys. Rev.* B **39** 4258
[19] Maki K and Thompson R S 1989 *Phys. Rev.* B **39** 2726
[20] Lihn H-T S, Wu S, Drew H D, Kaplan S, Qi Li and Fenner D B 1996 *Phys. Rev. Lett.* **76** 3810
[21] Allen J W and Mikkelson J C 1977 *Phys. Rev.* B **15** 2952
[22] Gurzhi R N 1958 *Zh. Eksp. Teor. Fiz.* **35** 965 (Engl. Transl. 1959 *Sov. Phys.–JETP* **8** 673)
[23] Campuzano J C, Jennings G, Faiz M, Beaulaigue L, Veal B W, Liu J Z, Paulikas A P, Vandervoort K,
    Claus H, List R S, Arko A J and Bartlett R J 1990 *Phys. Rev. Lett.* **64** 2308